Ali, M.; Ramirez Hoyos, P.; Nasir, S.; Nguyen, Q.; Ensinger, W.; Mafé, S. (2014). Current rectification by nanoparticle blocking in single cylindrical nanopores. Nanoscale. 6(18):10740-10745. doi:10.1039/c4nr02968b.

ARTICLE

Current Rectification by Nanoparticle Blocking in Single Cylindrical Nanopores

Mubarak Ali,[a,b,*] Patricio Ramirez,[c] Saima Nasir,[a,b] Quoc-Hung Nguyen,[a,b] Wolfgang Ensinger,[b] and Salvador Mafe[d,**]

Blocking of a charged pore by an oppositely charged nanoparticle can support rectifying properties in a cylindrical nanopore, as opposed to the usual case of a fixed asymmetry in the pore geometry and charge distribution. We present here experimental data and model calculations to confirm this fundamental effect. The nanostructure imaging and the effects of nanoparticle concentration, pore radius, and salt concentration on the electrical conductance-voltage (*G*-*V*) curves are discussed. Logic responses based on chemical and electrical inputs/outputs could also be implemented with a single pore acting as an effective nanofluidic diode. To better show the generality of the results, different charge states and relative sizes of the nanopore and the nanoparticle are considered, emphasizing those physical concepts that are also found in the ionic drug blocking of protein ion channels.

1. Introduction

Fundamental phenomena and potential applications of nanopores in liquid state ionics are based on current rectification, which is usually supported by asymmetrical pore shape and charge distributions.[1-4] We show here that blocking of a charged pore by a nanoparticle (NP) having opposite charge can give rectifying properties in a cylindrical nanostructure, as opposed to the usual case of asymmetric pore geometry and charge distributions. The pore is symmetric (cylindrical) but the external conditions are asymmetric because the solution containing NPs is introduced only on one side of the nanopore. We give a detailed experimental account of the effect together with simple model calculations. In particular, the nanostructure imaging and the effects of the NP concentration, pore radius, and salt concentration on the electrical conductance-voltage (*G*-*V*) curves are discussed for different charge states and pore and NP diameters. Pore blocking should be expected for the narrow pore while particle translocation occurs in the case of the wide pore.

We emphasize those physical concepts that are also found in the ionic drug blocking of protein ion channels.[5-8] This biophysical blocking depends on the applied voltage and the electrolyte concentration because of the mobile ions that are responsible for the Debye screening.[8] The long range electrical interaction between the charged species (NPs here) and the pore dictates the approaching to the pore entrance. Although specific short range interactions (e.g., hydrophobic and steric effects) could also be important for biomolecules. Some of the NP blocking characteristics described here are similar to those observed in the binding of antibiotic molecules to bacterial ion channels[5,6] and the blocking of channels involved in toxin infections by highly charged drugs.[7,8]

2. Experimental

The single cylindrical pores used in all experiments are obtained in polyethylene terephthalate (PET) membranes of thickness 12 μm irradiated with single swift heavy ions.[2] The membrane with the latent ion track is submitted to the symmetric track-etching technique for the preparation of cylindrical nanopores.[9,10] The heavy ion irradiation and subsequent chemical etching process used for the production of track-etched nanopores resulted in the cleavage of chemical bonds in the polymeric material (the etchant, NaOH, easily hydrolyses the partially charged ester bonds in the polymer chain). As a result carboxylic acid –COOH groups are generated on the inner pore walls. The density of carboxyl groups on the inner pore walls was[10] ~1 group nm^{-2}. The ionized carboxylate groups ($-COO^-$) impart negative fixed charges to the pore walls under our experimental conditions.

The pore surface charge characteristics can be switched from negative to positive through the chemical functionalization of the native carboxylic acid groups with ethylenediamine (EDA) via carbodiimide coupling chemistry.[1,2,9] Briefly, the –COOH groups on the pore surface were first converted into amine reactive PFP-esters by immersing the track-etched single-pore membranes in an ethanolic solution which contains a mixture of *N*-(3-dimethylaminopropyl)-*N'*-ethylcarbodiimide (EDC, 100 mM) and pentafluorophenol (PFP, 200 mM). The activation process was carried out for one hour. After washing with ethanol, the activated membranes were treated with ethylenediamine (EDA, 50 mM) solution prepared in ethanol for the amination of the channel surface. The PFP-reactive esters are hydrophilic in nature and rapidly react with the amine group of EDA molecule to form amide bonds. Subsequently, the modified membranes were washed first with ethanol and finally with deionised water.

Simultaneously with the single-pore membrane, a multi-pore membrane is prepared whose individual pore characteristics closely correspond to the single-pore sample because of the similar experimental procedure followed.[1,2,9,10] In the multi-pore membranes, Au nanowires are fabricated via replica method to image the internal pore geometry with field emission scanning electron microscopy (FESEM),[2,10] as shown in Figs. 1(a)-(c). The metallic replicas allow estimating the characteristics of the single cylindrical pore used in the experiments by inspecting cross-sections, pore tips, and axial fractures. These characteristics can be confirmed further by ionic transport experiments (e.g., current-voltage *I*-*V* curves).

The FESEM images corresponding to the cylindrical pores used in the experiments show the approximate symmetrical nature of the nanostructures. The images of the samples etched symmetrically for 5, 10 and 15 min. give the average pore diameters $2R$ = 30, 60, and 100 nm, respectively, in agreement with the effective diameters that can be obtained from ionic transport measurements.[2] The pore surface contains either carboxylic or amine moieties that are ionized (forms (-COO^- and -NH_3^+) in an aqueous solution at pH = 5.8. The polystyrene (PS) NPs of radius r = 30 nm approximately, as provided by the supplier (Bangs Laboratories, Fisher, IN), are also ionized (forms PS-(-COO^- and PS-NH_3^+) at pH = 5.8. The physico-chemical characteristics (surface charge, zeta potential, diameter variation and polydispersity index) of the NPs used here have been reported extensively in the literature.[11-14] The particles are added at a concentration c_p(particles mL^{-1}) in a KCl solution of known concentration c(mM). The two bathing solutions contain also 0.01 % v/v Tween 20 surfactant to avoid particle coagulation. Because the pore rectification can be influenced by the potential scan rate, the steady-state *I*-*V* curves are measured at scan rates low enough for the instantaneous current to be slave of the input potential signal, as explained previously in Refs. 2 and 15 and references therein.

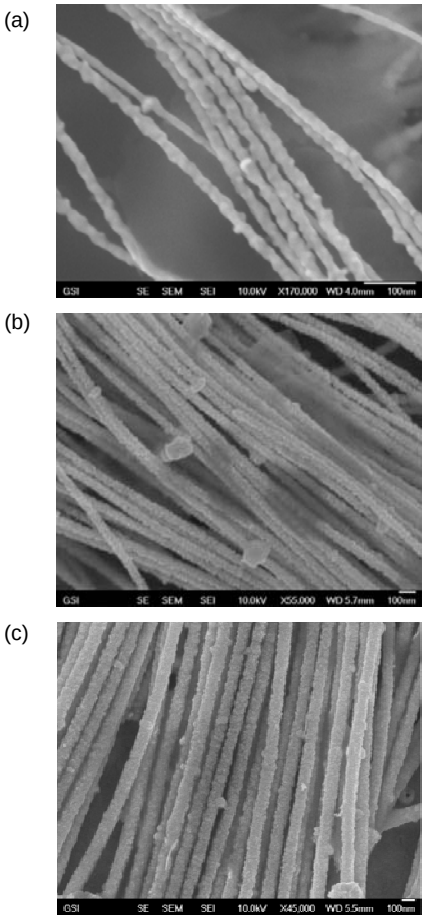

Fig. 1 FESEM images of the metallic replicas for the cylindrical, approximately symmetric pores used in the experiments. The fractures correspond to nanopores fabricated after 5 (a), 10 (b), and 15 (c) min of etching time resulting in approximate diameters ($2R$) of 30, 60, and 100 nm, respectively.

3. Results and discussion

Fig. 2(a) schematically shows the pore and the NP for different charge states. Stochastic particle capture using nanopores has previously been described.[11,12] However, we do not attempt here to obtain the particle characteristics from the individual events recorded in the current traces[11-13] but to characterize the steady-state rectification phenomena in Figs. 2(b) and 2(c). The relative sizes of the pore and the particle considered here provide a range of rectifications: significant blocking is expected for small pores ($R < r$) while particle translocation should occur for large pores ($r < R$). If the voltage sign is such that it forces the NP towards the pore, a significant drop in the current occurs because of blocking, and then pore rectification depends on the sign of the applied voltage V. Fig. 2(a) shows that blocking and unblocking can occur when the migration flow due to the particle surface charge and the electro-osmotic flow due the pore surface charge have the same direction.[11,12] Note the correspondence of the pore blocking mechanism in Fig. 2(a) with the current rectification observed in the *I*-*V* curves of Figs. 2(b) and 2(c). Note also that the rectification effect is lost if the NP and the pore have the same charge (Figs. 2(b)) because of the NP electrostatic exclusion.

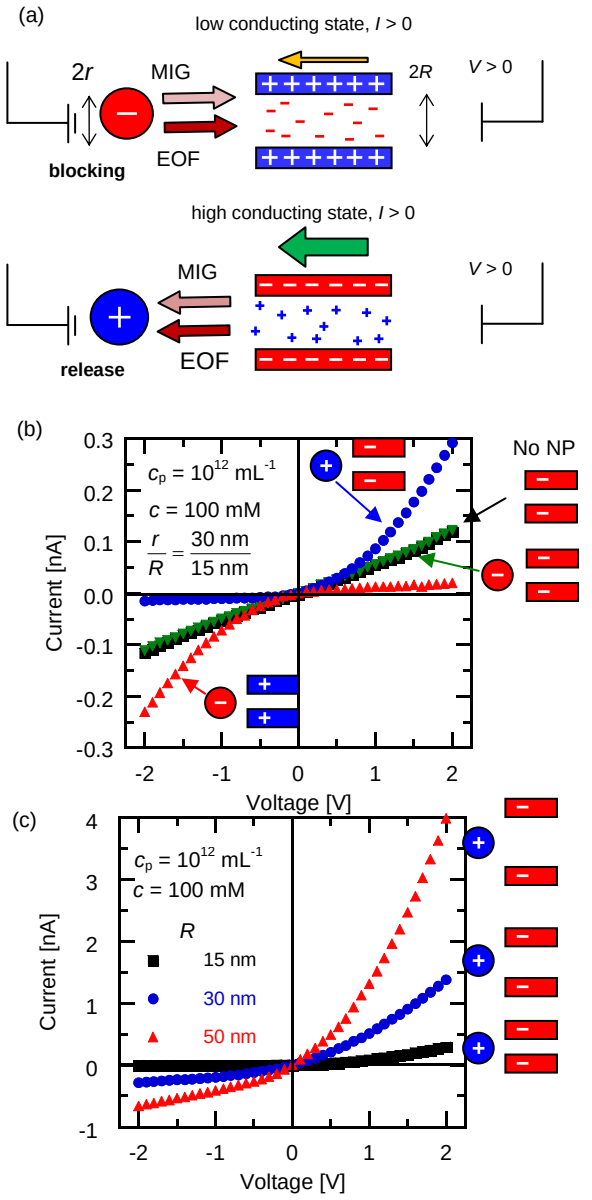

Fig. 2 The charged NP and the nanopore with the mobile charges compensating for the opposite charges fixed to the pore walls (a). We consider three experimental cases ($r > R$, $r \approx R$, and $r < R$) although only the case $r \approx R$ is shown in the figure for simplicity. The radii combinations r = 30 nm > R = 15 nm and $r \approx R$ = 30 nm allow significant pore blocking while the case $r < R$ = 50 nm permits particle translocation. The current $I > 0$ and its relative value (arrow) are shown for voltage $V > 0$ (the ground electrode is placed on the left side of the pore). Electro-osmotic (EOF) and migration (MIG) flows at the pore entrance are drawn out of the pore for the sake of clarity and should be reversed for $V < 0$. *I-V* curves for the negative (PS-COO^-) and positive (PS-NH_3^+) NPs and the oppositely charged pores. The curves for the negatively charged pore in absence of NPs and in presence of negatively charged NPs are also included (b). *I-V* curves for the positive NP and the oppositely charged pore parametrically in the pore radii R (c). The insets show the experimental conditions.

The NP transport rate is determined by three effects: diffusion, migration due to the externally imposed electric field that results from the application of an electric potential difference between the electrodes and, finally, the electro-osmotic flow due to movement of the charged liquid (this convective flow drags the charged NP). This transport problem has been studied for the cases of particle capture using nanopores[11,12] and ionic transport phenomena through fixed-charge membranes.[15-17] Assuming that the NP arrival rate to the pore mouth can be estimated from the steady-state flux of particles translocating through the pore when $r < R$,[11,16] we obtain:

$$\dot{N}_p = -A\left(\frac{D_p c_p}{\delta}\right)\left[\frac{\alpha V}{1-\exp(\alpha V)}\right], \quad \alpha = \left[z_p \frac{F}{RT} - \mathrm{sgn}(\sigma)\frac{\psi\delta}{D_p}\right] \qquad (1)$$

where $A = \pi R^2$ is the cross-section area of the pore, D_p is the NP diffusion coefficient, δ is the axial distance for transport through the pore, and σ is the charge density of the pore surface. The electro-osmotic velocity of the charged fluid can be made proportional to the applied potential by introducing the constant ψ which depends on the surface charge density and radius of the pore.[11,16] Finally, F, R and T are the Faraday and gas constants and the temperature, respectively, with $F = N_A e$ and $R = N_A k$ where N_A is the Avogadro constant, e is the proton charge, and k is the Boltzmann constant. In Eq. (1), the two contributions to α concern the potential gradient term and the fluid motion term. Note that the sign and absolute value of parameter α (and then the value of $\dot{N}_p$ at a given voltage V) is determined by the signs of the particle charge number z_p and the pore charge, with $\mathrm{sgn}(\sigma) = -1$ and $+1$ for the negative and positive pore, respectively.

Although Eq. (1) provides a qualitative picture of the NP transport, it does not allow the description of the current-voltage curves because of its extreme simplicity. Also, the high uncertainties in the parameters characteristic of the NP (z_p and D_p) and the pore (δ, σ, and ψ) in Eq. (1) preclude a quantitative analysis of the problem. Fig. 3 shows the NP arrival rate from the external solution to the pore mouth (see Fig. 2(a)) parametrically in α. This rate has been scaled to the purely diffusional rate $\dot{N}_0 = A\left(D_p c_p / \delta\right)$ to give the dimensionless ratio $\dot{N}_p / \dot{N}_0$ vs. V curves of Fig. 3.

The above ratio describing the NP arrival rate to the pore mouth should be related to the measured *I-V* curves: high arrival rates give frequent pore blocking (and then low current) while low rates leave the pore free for most of the time, allowing high currents. Pore blocking (low current I) and unblocking (high current I) can only occur when the particle and pore charges have opposite signs. In this case, the terms due to the particle (migration) and the pore surface (electro-osmotic flow) act together (see Fig. 2(a)) to increase the absolute value of α in Eq. (1) and Fig. 3. On the contrary, the sum of the migration and electro-osmotic terms tend to cancel one another, giving a low value of α in Eq. (1) and Fig. 3, if the NP and the pore surface have the same charge sign. This fact, together with the electrostatic exclusion of the NP from the pore, gives no rectification effects in this case.

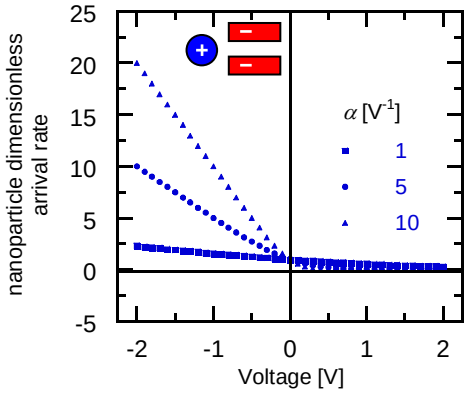

Fig. 3 NP arrival rate scaled to the purely diffusional rate, $\dot{N}_p / \dot{N}_0$, as a function of V. The different values of α are dictated by the relative signs and magnitudes of the migration and electro-osmotic terms in Eq. (1). Note the inverse correspondence between the positive NP arrival to (and blocking of) the pore mouth in this figure and the low ionic current I in Fig. 2(b) for $V < 0$.

Figs. 4(a) and (b) show the relative conductance change, $\Delta G/G_0$, for the case of the positive particle and the negative pore, where $G = I/V$ is obtained from the I-V curves and $\Delta G = G - G_0$ (G_0 is the pore conductance in the absence of NP).

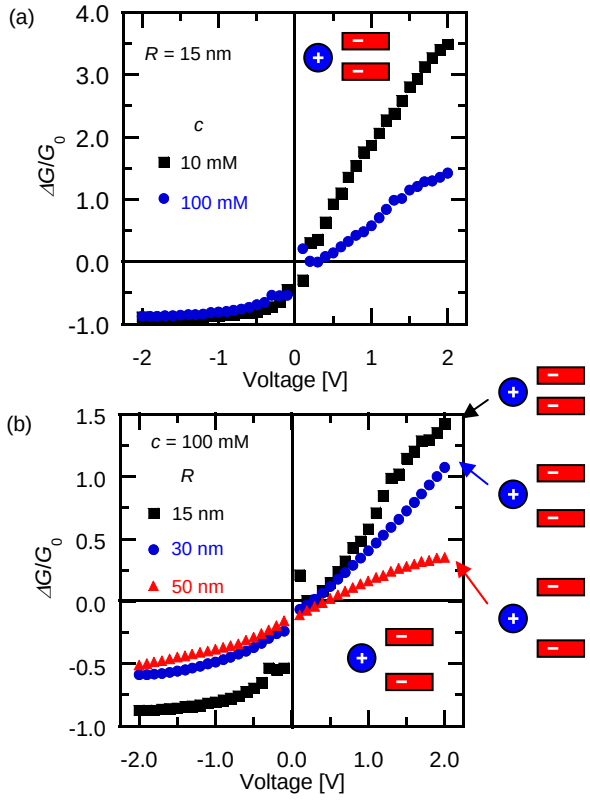

Fig. 4 The relative conductance change $\Delta G/G_0$ for the positive particle and the negative pore at different concentrations (a) and pore radii (b). The pore conductance, defined as $G = I/V$, is obtained from I-V curves similar to that of Fig. 2(b) and $\Delta G = G - G_0$, where G_0 is the pore conductance in absence of the NP. The inset shows the experimental conditions.

The transport experiments are conducted at pH = 5.8 for R = 15 nm and different aqueous solution concentrations (Fig. 4(a)) and for c = 100 mM and different pore radii (Fig. 4(b)). As expected from the generic I-V curve of Fig. 2(b), $\Delta G > 0$ for $V > 0$ while $\Delta G < 0$ for $V < 0$ in this case. The rectification is high for low electrolyte concentrations because of the low Debye screening (Fig. 4(a)). This fact enhances the electrostatic focusing[18] of the NP to the pore and subsequent blocking. Also, the rectification increases with decreasing the pore radius because of the increased pore blocking effect (Fig. 4(b)).

Figs. 5(a) and (b) show the effect of the NP concentration on the I-V and $\Delta G/G_0$-V curves in the case of the negative NP and the positive pore at pH = 5.8. Fig. 5(b) can be understood from the I-V curve of Fig. 2(b) showing that $\Delta G > 0$ for $V < 0$ while $\Delta G < 0$ for $V > 0$. Therefore, blocking and current reduction occurs only for $V > 0$ in this case. The high current obtained in absence of NP blocking ($V < 0$) is tentatively ascribed to the accumulation of charged NPs in the external pore entrance because of the electrical focusing. The charged NPs at the pore mouth tend to attract the small salt counterions,[19,20] compensating thus for the diffusion-limited conductance at low salt concentration. Recent experimental and theoretical work[13] with the same type of nanopores as those used here show indeed that hard sphere NPs can modulate ionic concentrations at the entrance of pores with micrometer-sized lengths.

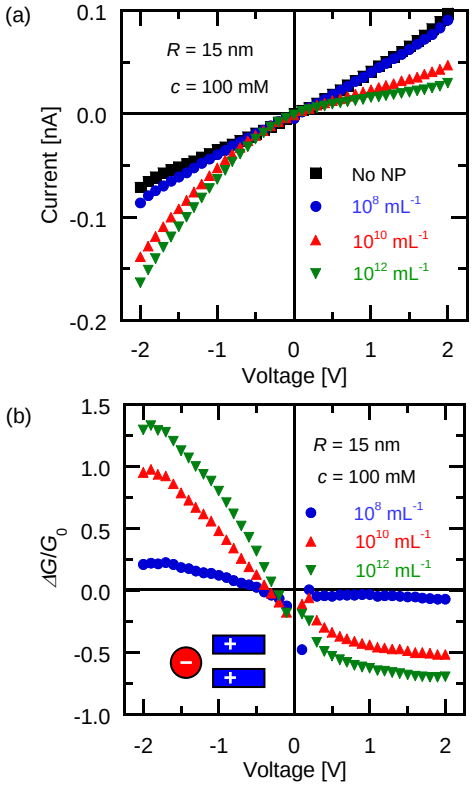

Fig. 5 I-V curves for the negative particle and the positive pore parametrically in the NP concentration (a). The relative change in the conductance, $\Delta G/G_0$, is obtained from the I-V curves of Fig. 5(a). The inset shows the experimental conditions and the relative sizes of the pore and particle.

A different, alternative explanation to the high current obtained in absence of NP blocking ($V < 0$) in Fig. 5(a) might be the adsorption of oppositely charged NPs on the first half (see Fig. 1(a) of the inner pore surface, thus creating a sort of bipolar structure across the pore length. However, it has been conclusively shown that polystyrene nanospheres remain approximately monodisperse (polydispersity index PDI < 0.1) in aqueous conditions (Figure 1 and Table 1 of Ref. 14). According to this low PDI, NP adsorption within the pore would be rather difficult when the NP radius is significantly greater than the pore radius, which is the case of the data in Fig. 5(a). For the opposite situation where the pore radius is significantly greater than the NP radius, irreversible adsorption of NPs to the inner pore walls should be especially noticeable because virtually all NPs would enter the pore (and eventually block it) in this case, regardless of their radii. This effect is not seen in the *I*-*V* curves of Fig. 2(c). Finally, we performed direct control experiments for the instantaneous current $I(t)$ *vs.* time t curves obtained for square wave voltages $V(t)$ of different amplitudes (data not shown) in presence of the NP. The output (current) as a function of the input (potential) signal did not show any apparent irreversible changes for short operating periods in the 100 s range.

Note also that the linear *I*-*V* curve obtained in the absence of NP (Fig. 5(a)) constitutes a proof of the pore symmetry (see also Figs. 1, 2(b), and 2(c)), confirming again the NP-induced rectification effect.

Finally, Fig. 6 shows the *I*-*V* curves for the negative pore and the positive particle either on the left or the right bathing solution. The single symmetrical pore may behave as two effective diodes, as indicated by the arrows, allowing different logic responses (the current is the output) according to the NP position with respect to the pore and the sign of the applied voltage (the inputs here).[21] The significant NP-induced rectification gives clearly discernible logical outputs and the reset function can be readily implemented by changing the sign of the applied voltage.

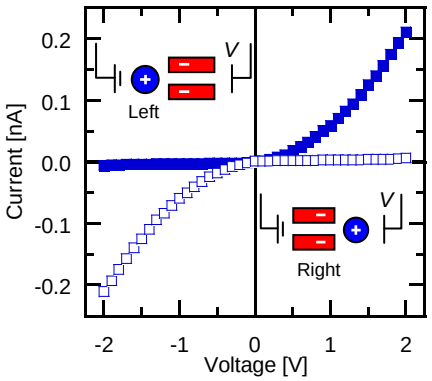

Fig. 6 *I*-*V* curves for the positive particle on the left (solid symbols, measured values) and right (open symbols, assumed values) of the negative pore. The experimental data are obtained for R = 15 nm, c = 10 mM, and the NP concentration $c_p = 10^{12}$ mL^{-1}. The NP position with respect to the pore and the sign of the applied voltage (inputs) give clearly discernible currents (output).

The rectification phenomena described in Figs. 2-6 reflect fundamental effects that are also characteristic of blocking in biological ion channels and membranes.[22] Indeed, the role of the complementary charges in the channel and the blocking ionic drug, the salt screening effect of the solution, the influence of the relative sizes of pore and molecule on the different blocking degrees, and the effects of the particle concentration and the applied potential have been discussed previously for the blocking of wide biological ion channels by antibiotic molecules and ionic drugs.[5-8] Note, in particular, the similarity between the increase in the blocked channel probability with the voltage $V > 0$ and the particle concentration observed in Fig. 3 of Ref. 8 and the decrease in the relative pore conductance of Fig. 5(b) here.

Conclusions

We have described an experimental approach to current rectification in pores which are symmetrical in the geometry and charge distribution. The results of Figs. 2-6 show a NP-induced rectification that can be easily achieved with different pore and particle characteristics for a wide range of NP concentrations. These facts suggest that the reported effect is robust and could find future applications by switching the nanopore-NP system between two states of different conductances.

The observed effects could be exploited in sensing and actuating applications by using multi-pore membranes[23] instead of single pores. In particular, average currents different from zero can be obtained with zero time-average external potentials[11,24] by switching a multi-pore membrane between the low and high conductance states caused by asymmetric blocking. This fact immediately suggests a method of rectifying fluctuating external signals to give a net charge flow.

Acknowledgements

M. A., S. N., Q.-H. N., and W. E. acknowledge the Beilstein-Institut, Frankfurt/Main, Germany, within the research collaboration NanoBiC. P. R. and S. M. acknowledge the Ministry of Economy and Competitiveness (project MAT2012-32084), FEDER, and the Generalitat Valenciana (project PROMETEO/GV/0069). The authors thank Prof. Dr. Christina Trautmann from GSI for support with the heavy ion irradiation experiments and an anonymous referee for helpful suggestions.

Notes and references

[a] Materials Research Dept., GSI Helmholtzzentrum für Schwerionen-forschung, Planckstrasse 1, D-64291, Darmstadt, Germany

[b] Technische Universität Darmstadt, Fachbereich Material- u. Geowissenschaften, Fachgebiet Materialanalytik, Petersenstraβe 23, D-64287 Darmstadt, Germany

[c] Dept. de Física Aplicada, Universitat Politécnica de València, E-46022 Valencia, Spain.

[d] Dept. de Física de la Terra i Termodinàmica, Universitat de València, E-46100 Burjassot, Spain.

*To whom correspondence should be addressed: E-mail: m.ali@gsi.de (M. Ali). Tel.: +49 6159 711866; Fax.: +49 6159 713266

**To whom correspondence should be addressed: smafe@uv.es. (S. Mafe). Tel.: +34 96 354 3119; Fax.: +34 96 354 3385

1 I. Vlassiouk and Z. Siwy, *Nano Lett.*, 2007, **7**, 55.
2 M. Ali, P. Ramirez, S. Mafe, R. Neumann and W. Ensinger, *ACS Nano*, 2009, **3**, 603.
3 J. Cervera, P. Ramirez, S. Mafe and P. Stroeve, *Electrochim. Acta*, 2011, **56**, 4504.
4 W. Guo, L. Cao, J. Xia, F.-Q. Nie, W. Ma, J. Xue, Y. Song, D. Zhu, Y. Wang and L. Jiang, *Adv. Funct. Mater.*, 2010, **20**, 1339.
5 E. M. Nestorovich, C. Danelon, M. Winterhalter and S. M. Bezrukov, *Proc. Natl. Acad. Sci. USA*, 2002, **99**, 9789.
6 S. Mafe, P. Ramirez and A. Alcaraz, *J. Chem. Phys.*, 2003, **119**, 8097.
7 V. A. Karginov, E. M. Nestorovich, M. Moayeri, S. H. Leppla and S. M. Bezrukov, *Proc. Natl. Acad. Sci. USA*, 2005, **102**, 15075.
8 M. Aguilella-Arzo, J. Cervera, P. Ramirez and S. Mafe, *Phys. Rev. E*, 2006, **73**, 041914 .
9 P.Y. Apel, I. V. Blonskaya, O. L. Orelovitch, B. A. Sartowska and R. Spohr, *Nanotechnology*, 2012, **23**, 225503.
10 M. Ali, P. Ramirez, Q. H. Nguyen, S. Nasir, J. Cervera, S. Mafe and W. Ensinger, *ACS Nano*, 2012, **6**, 3631.
11 S. Lee, Y. Zhang, H. S. White, C. C. Harrell and C. R. Martin, *Anal. Chem.*, 2004, **76**, 6108.
12 M. Davenport, K. Healy, M. Pevarnik, N. Teslich, S. Cabrini, A. P. Morrison, Z. S. Siwy and S. E. Létant, *ACS Nano*, 2012, **6**, 8366.
13 J. Menestrina, C. Yang, M. Schiel, I. Vlassiouk and Z. S. Siwy, *J. Phys. Chem. C*, 2014, **118**, 2391.
14 T. Xia, M. Kovochich, J. Brant, M. Hotze, J. Sempf, T. Oberley, C. Sioutas, J. I. Yeh, M. R. Wiesner and A. E. Nel, *Nano Lett.* **6** (2006) 1794.
15 P. Ramirez, V. Gomez, M. Ali, W. Ensinger and S. Mafe, *Electrochem. Commun.*, 2013, **3**, 137.
16 R. Schögl, *Ber. Bunsenges. Phys. Chem.*, 1966, **70**, 400.
17 J. Pellicer, S. Mafe and V. M. Aguilella, *Ber. Bunsenges. Phys. Chem.*, 1986, **90**, 867.
18 M. Wanunu, W. Morrison, Y. Rabin, A. Y. Grosberg and A. Meller, *Nat. Nanotechnol.*, 2010, **5**, 160.
19 M. X. Macrae, S. Blake, M. Mayer and J. Yang, *J. Am. Chem. Soc.* 2010, **132**, 1766.
20 M. Tagliazucchi, Y. Rabin and I. Szleifer, *ACS Nano*, 2013, **7**, 9085.
21 P. Ramirez, M. Ali, W. Ensinger and S. Mafe, *Appl. Phys. Lett.*, 2012, **101**, 133108.
22 B. Hille, Ion Channels of Excitable Membranes (Sinauer, Sunderland, 1992).
23 M. Ali, S. Nasir, P. Ramirez, J. Cervera, S. Mafe and W. Ensinger, *J. Phys. Chem. C*, 2013, **117**, 18234.
24 M. Ali, P. Ramirez, S. Nasir, Q.-H. Nguyen, W. Ensinger and S. Mafe, *Appl. Phys. Lett.*, 2014, **104**, 043703.